JASA ARTICLE

Robust sparse reconstruction of attenuated acoustic field with unknown range of source

Yongfei Li,[1,a] Ruiming Guo,[2] Thierry Blu,[2] and Hangfang Zhao[1,b]
[1]College of Information Science and Electronic Engineering, Zhejiang University, Hangzhou, Zhejiang 310007, China
[2]Department of Electronic Engineering, Chinese University of Hong Kong, Hong Kong 999007, China

ABSTRACT:
In this paper, we present a gridless algorithm to recover an attenuated acoustic field without knowing the range information of the source. This algorithm provides the joint estimation of horizontal wavenumbers, mode amplitudes, and acoustic attenuation. The key idea is to approximate the acoustic field in range as a finite sum of damped sinusoids, for which the sinusoidal parameters convey the ocean information of interest (e.g., wavenumber, attenuation, etc.). Using an efficient finite rate of innovation algorithm, an accurate recovery of the attenuated acoustic field can be achieved, even if the measurement noise is correlated and the range of the source is unknown. Moreover, the proposed method is able to perform joint recovery of multiple sensor data, which leads to a more robust field reconstruction. The data used here are acquired from a vertical line array at different depths measuring a moving source at several ranges. We demonstrate the performance of the proposed algorithm both in synthetic simulations and real shallow water evaluation cell experiment 1996 data.
https://doi.org/10.1121/10.0016497
(Received 19 June 2022; revised 22 November 2022; accepted 23 November 2022; published online 14 December 2022)
[Editor: Peter Gerstoft] Pages: 3523–3534

I. INTRODUCTION

In a shallow water environment, normal mode theory has been widely used to describe the propagation characteristics of underwater sound,[1] providing a sparse representation of the acoustic field.[2–4] The information of interest, such as horizontal wavenumbers, are encoded in the spatial distribution of the attenuated acoustic field, which plays an important role in a wide variety of ocean applications, such as localization,[5–7] geoacoustic inversion,[8,9] time reversal mirror,[10,11] tomography,[12,13] etc. Accurate and robust recovery of the acoustic field, including the estimation of horizontal wavenumbers, mode amplitudes, and propagation attenuations, is at the heart of underwater acoustics.

In this study, a gridless algorithm is proposed to recover an attenuated acoustic field without knowing the range of the source. The key idea is to approximate the attenuated acoustic field (in range) as a finite sum of damped sinusoids in which the information of interest is encrypted. An efficient high-resolution sparse algorithm, the finite rate of innovation (FRI) algorithm,[14,15] is used to accurately retrieve the damped sinusoidal parameters (complex wavenumbers plus amplitudes). The data used in this paper are acquired from a moving source at several ranges and recorded by a vertical line array (VLA) at different depths.

By approximating the acoustic field as a finite sum of damped sinusoids, we achieve acoustic field reconstruction via a parametric model fitting, for which its parameters are inextricably linked to wavenumber estimation. In other words, wavenumber estimation is a classical and important topic in underwater acoustic applications. It has been thoroughly studied in two experimental settings, including horizontal line arrays (HLAs) and fixed source settings[2,16] or VLAs[4,17] and mobile source settings.[3] Usually, the problem is formulated as a spatial spectral estimation, which leads to several well-known algorithms, such as spatial Fourier and Hankel transform.[16,18] They obtain the wavenumber spectrum by integrating the acoustic pressure over range. However, a large range aperture (i.e., a very long HLA or synthetic aperture) is needed to guarantee the resolution of adjacent wavenumbers, which is infeasible in practice.

In the past few decades, many high-resolution methods have been proposed to estimate wavenumbers. Among them, Prony's method,[19] autoregressive spectral estimators,[20,21] and subspace-based methods[22,23] are the most common. Although these standard high-resolution techniques can improve the spatial resolution effectively, strict assumptions on the measurement noise are still required, e.g., additive white Gaussian noise. These assumptions are not in line with the reality, leading to inaccurate acoustic field reconstruction.

Taking advantage of the sparsity of the propagating modes, the conventional compressed sensing (L2-CS) is proposed to handle wavenumber estimation in underwater acoustics and has attained good performance in practical applications.[2] However, the conventional L2-CS method approximates a continuous parameter space with a finite discretized grid. Hence, inaccuracy

[a]Present address: Nanjing Research Institute of Electronics Technology, Nanjing, Jiangsu 210013, China.
[b]Also at: the Key Laboratory of Ocean Observation-Imaging Testbed of Zhejiang Province, Zhoushan, Zhejiang 316021, China. Electronic mail: hfzhao@zju.edu.cn

occurs when the parameters are not on the grid.[24–26] To address this issue, the Atomic-CS method is developed to estimate the parameters in continuous domain by solving a semi-definite programming problem. It overcomes basis mismatch and shows its superior performance.[3,27,28]

Although these high-resolution techniques mentioned above have achieved great success, there are still unresolved issues in practice. Most wavenumber estimation methods rely on the range information of the source to handle the transmission loss (TL), e.g., cylindrical spreading.[2,3,6,18,21,22,29,30] They are not robust enough in the absence of the source range knowledge (see Fig. 1). Moreover, the computational cost of most high-resolution algorithms [e.g., L2-CS, atomic-CS, estimating signal parameter via rotational invariance technique (ESPRIT), multiple signal classification (MUSIC)] scales with the number of range samples and sensors, which is time-consuming in practical applications.[14,15]

As for the complex wavenumber/frequency estimation, our postulate is that *any* sum of damped sinusoids that fits our data within a predefined mean square error (MSE) is a valid solution to our problem, i.e., we do not aim to minimize the MSE between the recovered field and measurements. In other words, we do not assume any statistical model about noise, but only ensure that the reconstruction MSE is within the noise variance (i.e., "MSE budget"). Moreover, this MSE criterion also provides a robust way to determine the order of the model: the smallest number of sinusoids for which this sum of damped sinusoids is a valid solution.

Compared with the existing high-resolution methods, the proposed method does not require *a priori* range of the source to compensate for the cylindrical spreading, instead, using the damping factor to approximate the TL (caused by the cylindrical spreading, absorption of medium, and absorption at the interface). In this case, the attenuated acoustic field can be approximated as a finite sum of damped sinusoids—a parametric model (i.e., wavenumbers, mode amplitudes, and damping factors). By fitting the measurements with the parametric model, we show that our algorithm works accurately on challenging acoustic field recovery in both simulations and real SWellEx-96 data regardless of model mismatch (see Secs. IV and V). Moreover, our algorithm is very efficient, in that it is able to process large amounts of data within a short time (see Sec. IV A 4).

II. PROBLEM FORMULATION USING FRI

A. Signal model

The normal mode theory is widely used for low-frequency sound propagation in shallow water. Given a single frequency f_0 point source at depth z_s in a range-independent ocean waveguide environment, the pressure is received by a sensor at depth z_r and range r. The acoustic field can be expressed by a sum of M propagative modes

$$s(r, z_r) = A_0 \sum_{m=1}^{M} \phi_m(z_s)\phi_m(z_r)\frac{e^{jk_{r,m}r}}{\sqrt{k_{r,m}r}}, \tag{1}$$

where $A_0 = S_0(f_0)e^{j\pi/4}/\sqrt{8\pi}\rho(z_s)$ and M is the number of propagative modes. $k_{r,m}$ and ϕ_m are horizontal wavenumber and mode depth function of m-th mode. The quantity $S_0(f_0)$

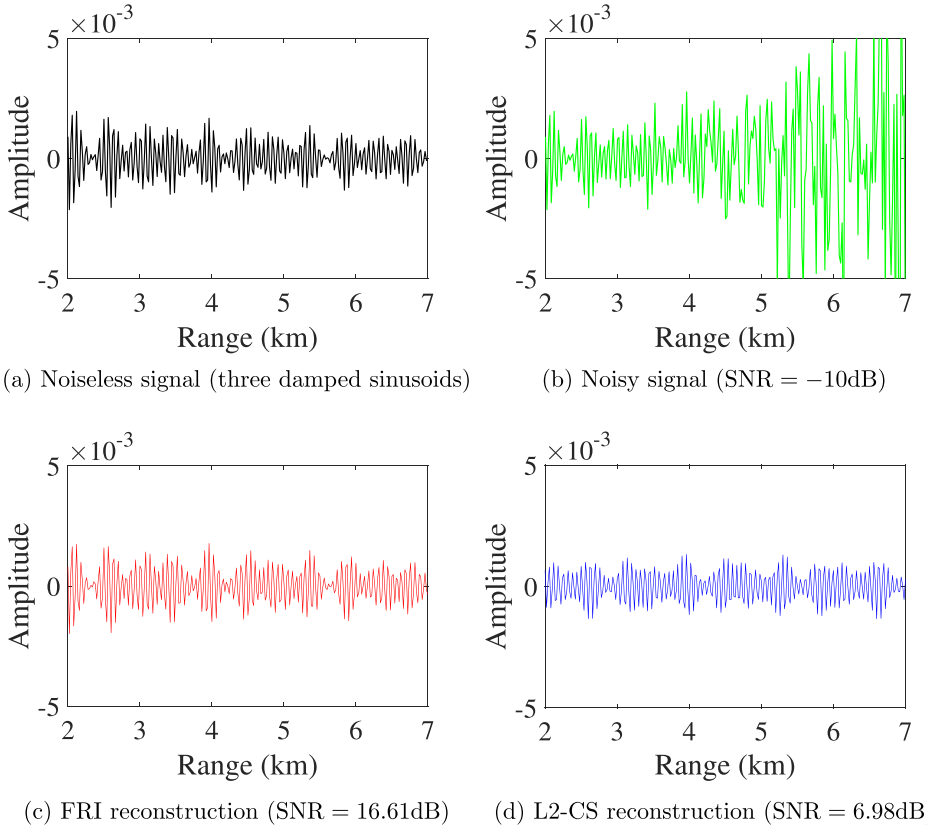

(a) Noiseless signal (three damped sinusoids) (b) Noisy signal (SNR = −10dB)

(c) FRI reconstruction (SNR = 16.61dB) (d) L2-CS reconstruction (SNR = 6.98dB)

FIG. 1. (Color online) Acoustic field reconstruction from single-sensor noisy measurements (colored noise, SNR = −10 dB) without knowing range of the source. In contrast to FRI, standard high-resolution wavenumber estimation techniques like L2-CS are not robust enough to achieve an accurate recovery in practice. The energy of signal noise increases rapidly with range. In this figure, we plot the range of source for ease of performance evaluation.

https://doi.org/10.1121/10.0016497

denotes the source spectrum at frequency f_0 and $\rho(z_s)$ is the water density at depth z_s.

Given an L-element VLA at depths z_0, z_1,…, z_{L-1}, the sound pressure at each sensor is measured over a constant time interval with ranges r_0, r_1,…, r_{N-1}. Note that the pressure is uniformly sampled with sampling interval Δr, i.e., $r_n = r_0 + n\Delta r$. With known range of the source r_0, the above is a classical wavenumber estimation problem, and some standard high-resolution methods, e.g., L2-CS[2] and Atomic-CS,[3] rely on the range of the source to compute the contribution of the attenuation (i.e., cylindrical spreading $1/\sqrt{r_n}$). However, these methods are not robust enough in the absence of the range of the source r (see Fig. 1).

In practice, when r_0 is large enough, the pressure of the l-th sensor can be approximated accurately as a finite sum of damped sinusoids (FRI signal), and it can be rewritten by

$$\begin{aligned} s_{n,l} &= A_0 \sum_{m=1}^{M} \phi_m(z_s)\phi_m(z_{r,l}) \frac{e^{jk_{r,m}r_n}}{\sqrt{k_{r,m}r_n}} \\ &\simeq \sum_{m=1}^{M} c_{m,l} e^{(-\alpha_m + j\omega_m)n}, \\ &\quad n = 0, 1, \ldots, N-1 \text{ and } l = 0, 1, \ldots, L-1, \end{aligned} \tag{2}$$

where FRI amplitude $c_{m,l} = A_0\phi_m(z_s)\phi_m(z_{r,l})e^{j\theta_m(r_0)}/\sqrt{k_{r,m}}$ is proportional to the amplitude of m-th mode of l-th sensor. $\theta_m(r_0)$ is the phase term associated with r. FRI frequency $\omega_m = k_{r,m}\Delta r$ is proportional to the horizontal wavenumber. α_m represents the damping factor to compensate for the cylindrical spreading. Notably, the exponential attenuation $e^{-\alpha_m r}$ is used to approximate the cylindrical spreading $1/\sqrt{r}$ in Eq. (2). This makes it possible to recover the acoustic field using the robust FRI algorithm without knowing the range of the source r (i.e., r_0 is unknown). By approximating the acoustic field as a finite sum of damped sinusoids, we achieve acoustic field reconstruction via a parametric model fitting. We highlight again, in this paper, what is known to us is only the spatial sampling interval Δr, in the absence of the range of source r.

In fact, the damping factor α_m contains the contributions of all factors that cause acoustic field attenuation (e.g., the cylindrical spreading, absorption of the medium, absorption at the interface, etc). Note that ω_m and α_m denote the wavenumber and damping factor of the m-th sinusoid, which are common to all sensors. However, the amplitudes $c_{m,l}$ of these damped sinusoids are expected to vary across all sensors.

In Eq. (2), it provides a parametric sparse representation, which makes it possible to accurately recover the acoustic field when the range r is unknown. As suggested by Eq. (2), this problem can be formulated as a high-resolution multi-sensor (complex) wavenumber estimation, which has been thoroughly studied.[3,28,31] However, these high-resolution techniques are not robust enough to retrieve the model parameters due to correlated noise corruption, signal distortion and model mismatch (see Fig. 1). For this reason, we use an FRI (sparse) approximation approach instead. By fitting the acoustic data in the sparse domain, we will see that accurate retrieval of the information encoded within the acoustic data are possible, despite the strong noise corruption.

B. FRI approximation

FRI approximation consists, first, in transforming the damped sinusoidal signal (i.e., acoustic field) into a sparse signal. More specifically, by computing the discrete Fourier transform (DFT) of a sum of M damped sinusoids, we get a sum of Dirichlet sinc kernels, which finally can be expressed in the form of a ratio of two polynomials in $d = e^{-j(2\pi n/N)}$ (Ref. 14),

$$\begin{aligned} \hat{s}_{n,l} &= \sum_{n'=0}^{N-1} s_{n',l} e^{-j(2\pi n' n/N)} \\ &= \underbrace{\sum_{n'=0}^{N-1} \sum_{m=1}^{M} c_{m,l} e^{(-\alpha_m + j\omega_m)n'} e^{-j(2\pi n' n/N)}}_{\text{sum of geometric progression}} \\ &= \sum_{m=1}^{M} c_{m,l} \frac{1 - e^{N(-\alpha_m + j\omega_m)}}{1 - z e^{(-\alpha_m + j\omega_m)}} \\ &= \frac{P_{M-1,l}(d)}{Q_M(d)}, \end{aligned} \tag{3}$$

where the numerator, $P_{M-1,l}(d)$, and the denominator, $Q_M(d)$, are polynomials of degree $M-1$ and M, respectively. The parameters ω_m and α_m, common to all the sensors, are uniquely determined by a unique polynomial $Q_M(d)$, whereas the different amplitudes of each sensor result in different $P_{M-1,l}(d)$, $l = 0, \ldots, L-1$.

As a result, in noisy conditions, the sparse reconstruction of multi-sensor damped sinusoids can be formulated as the following least-square fitting problem according to Parseval's identity:

$$\min_{Q_M, P_{M-1,l}} \sum_{l=0}^{L-1} \sum_{n=0}^{N-1} \left| \hat{s}_{n,l} - \frac{P_{M-1,l}\left(e^{-j2\pi n/N}\right)}{Q_M\left(e^{-j2\pi n/N}\right)} \right|^2. \tag{4}$$

Once the denominator Q_M and numerator P_M are retrieved, the wavenumber ω_m and damping factor α_m are given by

$$\begin{aligned} \omega_m &= \text{Real}(j \log(d_m)), \\ \alpha_m &= \text{Real}(\log(d_m)), \end{aligned} \tag{5}$$

where d_m denotes the m-th zeros of Q_M. The amplitude $c_{m,l}$ can be calculated by

$$c_{m,l} = -\frac{N z_m^{-1} P_{m-1,l}(z_m)}{\left(1 - z_m^{-N}\right) Q'_M(z_m)}. \tag{6}$$

However, the minimization in Eq. (4) is a non-convex problem, and difficult to solve directly. In order to find a good approximation of the solution of Eq. (4), we choose

the linear iterative strategy[14,32] to make the MSE in Eq. (4) decrease fast,

$$\min_{Q_M^{(i)},P_{M-1,l}^{(i)}} \sum_{l=0}^{L-1}\sum_{n=0}^{N-1}\left|\frac{Q_M^{(i)}(\mathrm{e}^{-j2\pi n/N})\hat{s}_{n,l}-P_{M-1,l}^{(i)}(\mathrm{e}^{-j2\pi n/N})}{Q_M^{(i-1)}(\mathrm{e}^{-j2\pi n/N})}\right|^2$$
$$\text{subject to } \int_0^{2\pi}\overline{Q_M^{(0)}(e^{j\bar{\theta}})}Q_M^{(i)}(e^{-j\theta})d\theta=2\pi, \tag{7}$$

where Q_M^i and P_M^i denote the results of the i-th iteration. Q_M^0 is the initialization. The candidates for denominator Q_M are obtained by solving iteratively for $i=1\cdots i_{\max}$. $\int_0^{2\pi}\overline{Q_M^{(0)}(e^{j\bar{\theta}})}Q_M^{(i)}(e^{-j\theta})d\theta=2\pi$ denotes the linear constraint to attain an unique solution to Eq. (7). We construct adequate candidates and pick the one for which the MSE between the recovered field and measurements is the smallest.

As soon as the fitting error is less than a predefined MSE budget, the approximate solution obtained is sufficiently accurate in practice. We reinitialize $Q_M^{(0)}$ and repeat the process, if no iterates gives a fitting error smaller than the MSE budget after the maximum number of iterations ($=i_{\max}$) has been reached. In fact, FRI performs exact model-fitting in a domain where the signal is sparse, i.e., the signal energy is highly concentrated that provides stronger robustness against noise corruption. The detailed algorithm implementation is shown in Sec. III.

C. MSE budget criterion

In underwater acoustic applications, the measurement noise is correlated and colored, hence a white noise assumption is not realistic. Moreover, only limited noise statistics, such as mean and variance, is available in practice, which makes it unfeasible to develop a reliable statistical model of the measurement noise. As a result, instead of minimizing the MSE between the recovered field and measurements, our postulate is that any sum of M damped sinusoids is a valid solution to our problem as soon as the MSE criterion

$$\mathrm{MSE}_{\mathrm{rec},l}\le\sigma_l^2,\quad l=0,\ldots,L-1 \tag{8}$$

is satisfied, where $\mathrm{MSE}_{\mathrm{rec},l}$ is the MSE between the l-th sensor measurements and the recovered field. σ_l^2 is the noise margin of the l-th sensor, assumed to be known (e.g., obtained from pre-measurements when there is no source in the observation area).

D. Model order

The other problem is the estimation of model order. With the MSE budget criterion, a natural way to determine the order of the model is to choose the smallest value of M for which the fitting error is no larger than the MSE budget. An efficient and fast implementation of this parsimony principle uses a line dichotomous search that is explicitly described in Ref. 33.

III. ALGORITHM IMPLEMENTATION

In this section, we give the detailed algorithm implementation. First, the polynomials in Eq. (3) can be expressed in vector form,

$$\{P_{M-1,l}(e^{-j(2\pi n/N)})\}_{n=0}^{N-1}=\mathbf{U}_{N,M}\mathbf{p}_l,$$
$$\{Q_M(e^{j-(2\pi n/N)})\}_{n=0}^{N-1}=\mathbf{U}_{N,M+1}\mathbf{q}, \tag{9}$$

where $\mathbf{p}_l\in\mathbb{Z}^{M\times1}$ and $\mathbf{q}\in\mathbb{Z}^{(M+1)\times1}$ denote the polynomial coefficients of $P_{M-1,l}(d)$ and $Q_M(d)$, respectively. $\mathbf{U}_{N,N'}=[e^{j(2\pi n'n/N)}]$ is the $N\times N'$ DFT matrix.

Now, we define $\tilde{\mathbf{p}}=[\mathbf{p}_0^T\cdots\mathbf{p}_{L-1}^T]^T\in\mathbb{Z}^{LM\times1}$ by stacking all the vectors $\mathbf{p}_l$, $\mathbf{R}_{i-1}=\mathrm{diag}\{\mathbf{U}_{N,M+1}\mathbf{q}_{i-1}\}\in\mathbb{Z}^{N\times N}$ denotes the diagonal matrix made of the vector $\mathbf{U}_{N,M+1}\mathbf{q}_{i-1}$, and $\hat{\mathbf{s}}_l=[\hat{s}_{0,l}\cdots\hat{s}_{N-1,l}]^T\in\mathbb{Z}^{N\times1}$ is the data vector of the l-th sensor (the raw data of each sensor are normalized by their noise margin σ_l to reduce the number of iterations needed to satisfy the MSE criterion.). Applying the linear constraint $\mathbf{q}_0^H\mathbf{q}=1$ ($\mathbf{q}_0$ is randomly initialized) to ensure the uniqueness of the solution, Eq. (7) can be rewritten in matrix form

$$\min_{\mathbf{q}_i,\tilde{\mathbf{p}}_i}||\mathbf{A}_{i-1}\mathbf{q}_i-\mathbf{B}_{i-1}\tilde{\mathbf{p}}_i||^2\ \text{ s.t. }\ \mathbf{q}_0^{\mathrm{H}}\mathbf{q}_{\mathrm{i}}=1, \tag{10}$$

where $\mathbf{A}_{i-1}$ and $\mathbf{B}_{i-1}$ are defined as

$$\mathbf{A}_{i-1}=\begin{bmatrix}\mathrm{diag}\{\hat{\mathbf{s}}_0\}\\ \mathrm{diag}\{\hat{\mathbf{s}}_1\}\\ \vdots\\ \mathrm{diag}\{\hat{\mathbf{s}}_{L-1}\}\end{bmatrix}(\mathbf{R}_{i-1})^{-1}\mathbf{U}_{N,M+1}\in\mathbb{Z}^{NL\times(M+1)},$$
$$\mathbf{B}_{i-1}=\mathbf{I}_L\otimes\left(\mathbf{R}_{i-1}^{-1}\mathbf{U}_{N,M}\right)\in\mathbb{Z}^{NL\times M}, \tag{11}$$

where $\mathbf{I}_L$ denotes the $L\times L$ identity matrix and $\otimes$ denotes the Kronecker product. Assume that $\mathbf{q}_{i-1}$ have been calculated at iteration $i-1$, the minimization problem at iteration i in Eq. (10) results in the update

$$\begin{bmatrix}\mathbf{q}_i\\ -\tilde{\mathbf{p}}_i\end{bmatrix}=\lambda\left([\mathbf{A}_{i-1},\mathbf{B}_{i-1}]^{\mathrm{H}}[\mathbf{A}_{i-1},\mathbf{B}_{i-1}]\right)^{-1}\begin{bmatrix}\mathbf{q_0}\\ 0\end{bmatrix}, \tag{12}$$

where λ is such that $\mathbf{q}_0^H\mathbf{q}_i=1$ is satisfied. In general, 5 random initializations and $i_{\max}=20$ are sufficient to obtain a solution that fits the data within the expected noise level $\sigma_{\mathrm{noise}}^2$. The main procedure is summarized in Algorithm 1.

IV. SIMULATION

In this section, our FRI approximation algorithm is evaluated in various conditions. To perform these tests, the algorithm is implemented in MATLAB 2019b on a computer with an i7-7700 CPU and 16 G of RAM. For comparison purposes, the L2-CS technique is implemented in a classical form of minimizing l_1-norm with l_2-norm constraint[2] and Atomic-CS is implemented in a form of minimizing atomic norm,[3] using the CVX (convex) toolbox in the MATLAB

https://doi.org/10.1121/10.0016497

ALGORITHM 1: FRI approximation algorithm.

Input: Multi-sensor measurements $\{s_{n,l}\}_{n=0\cdots N-1}^{l=0\cdots L-1}$,
noise level $\{\sigma_l^2\}_{l=0\cdots L-1}$.
for *loop* = 1 to *max. initializations* **do**
  Initialize $\mathbf{q}$ with a random vector $\mathbf{q}_0$;
  for $i = 1$ to *max. iterations* **do**
    Build the matrices involved in (10) with $\mathbf{q}_{i-1}$, such as $\mathbf{A}_{i-1}$, $\mathbf{B}_{i-1}$, and etc;
  Update $\mathbf{q}_i$ and $\tilde{\mathbf{p}}_i$ by solving (10);
    if $\sum_{n=0}^{N-1} |\hat{s}_{n,l} - \frac{P_{M-1,l}(d)}{Q_M(d)}|^2 \le \sigma_l^2$, for all l **then**
      Terminate all loops;
    end if
  end for
end for
$\mathbf{q} = \mathbf{q}_i$, $\tilde{\mathbf{p}} = \tilde{\mathbf{p}}_i$;
Calculate $\{\omega_m\}_{m=1\cdots M}$, $\{\alpha_m\}_{m=1\cdots M}$ and $\{c_{m,l}\}_{m=1\cdots M}^{l=0\cdots L-1}$ using (5) and (6).
Output: The frequencies $\{\omega_m\}_{m=1\cdots M}$, damping factor $\{\alpha_m\}_{m=1\cdots M}$, amplitudes $\{c_{m,l}\}_{m=1\cdots M}^{l=0\cdots L-1}$, and recovered signal $\{s_{n,l}\}_{n=0\cdots N-1}^{l=0\cdots L-1}$.

environment. In the situation of multi-sensor acoustic measurements, ESPRIT and MUSIC are usually based on the covariance matrix.[22]

Note that, for atomic-CS, the wavenumbers or frequencies are estimated by finding the roots of the $2(N-1)$-order polynomial on the unit circle.[3,27,28] However, due to the effect of attenuation, the ground truths (complex wavenumbers or frequencies) do not fall on the unit circle. Therefore, atomic-CS is not very suitable for dealing with the damped sinusoids in this paper. For comparison purposes, we find M roots nearest to the unit circle as the estimated results.

In order to evaluate the algorithm performance, the SNR of multi-sensor signal is defined as

$$\mathrm{SNR} = 10\log \frac{\sum_{l=0}^{L-1} ||\mathbf{s}_l||^2}{\sum_{l=0}^{L-1} \sigma_l^2}, \tag{13}$$

where $\mathbf{s}_l$ denotes the signal samples of l-th sensor and σ_l^2 is the corresponding noise level.

A. Performance analysis

1. Performance curve

In the presence of additive white Gaussian noise, the Cramér-Rao lower bounds (CRLB)[34,35] provides the best performance in statistical sense (under unbiasedness assumption). To test the performance of multi-sensor FRI approximation, the root mean square error (RMSE) of frequency is given by

$$\mathrm{RMSE} = \sqrt{\mathscr{E}\left(\frac{1}{M}\sum_{m=1}^{M}(\omega_m - \hat{\omega}_m)^2\right)}, \tag{14}$$

where ω_m is the ground truth, and $\hat{\omega}_m$ is the estimated frequency. The RMSE of the damping factor α_m is defined in a similar way. For the damped sinusoid signal, the CRLBs for the frequency ω and damping factor α are given by[34,35]

$$\sigma_\omega^2 = \sigma_\alpha^2 = \frac{(1-\gamma^2)^3(1-\gamma^{2N})}{2L\rho_0\left[-N^2\gamma^{2N}(1-\gamma^2)^2 + \gamma^2(1-\gamma^{2N})^2\right]}, \tag{15}$$

where ρ_0 is the SNR and $\gamma = |e^{-\alpha}|$.

Figures 2(a) and 2(b) display the RMSEs of frequency and damping factor with regard to SNR, respectively, for the case of a single damped sinusoid sampled at 21 locations in 10 sensors. The computed RMSE curves of our FRI method reach the CRLBs[34,35] (up to SNR = −5dB), which demonstrates its good performance. L2-CS and MUSIC can only deal with real-valued frequencies, which cannot meet the requirements of ocean acoustic applications. As can be seen in Fig. 2, other techniques like ESPRIT and atomic-CS are not sufficiently robust to retrieve complex-valued frequencies from noisy data.

2. Multi-sensor enhancement

In this part, the multi-sensor enhancement of our FRI algorithm is investigated. Figures 3(a) and 3(b) present the

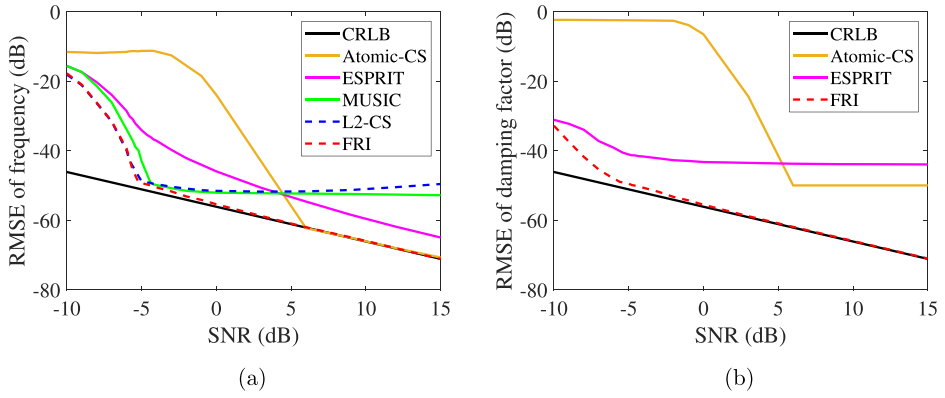

FIG. 2. (Color online) Comparing the performance curve (averages over 5000 realizations) of ESPRIT, MUSIC, L2-CS, atomic-CS and FRI with CRLB. (a) RMSE of frequency. (b) RMSE of damping factor. $M = 1$ damped sinusoid ($\omega_1 = 0.75, \alpha_1 = 0.02$), $N = 21$ samples, and $L = 10$ sensors (additive white Gaussian noise). FRI approaches the CRLBs up to a low SNR of −5 dB. Common techniques such as L2-CS and MUSIC, can only work with undamped data, which do not meet the requirements of the recovery of attenuated acoustic field. Other techniques like ESPRIT and Atomic-CS are not sufficiently robust in the presence of noise.

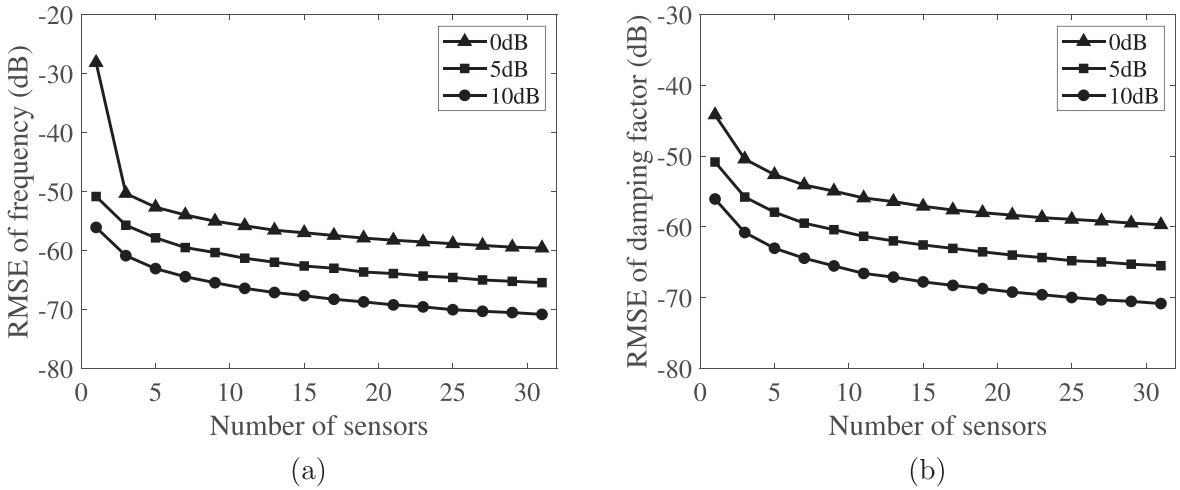

FIG. 3. RMSE (averages over 10 000 realizations) for FRI reconstruction versus the number of sensors with SNR = 0, 5, and 10 dB. (a) RMSE of frequency. (b) RMSE of damping factor. Note that $M = 1$ damped sinusoid, and $N = 21$ samples (additive white Gaussian noise).

RMSEs of frequency and damping factor versus the number of sensors with SNR = 0, 5, and 10 dB. RMSEs decrease as the number of sensors increases, which proves that multi-sensor samples can effectively improve the accuracy of estimation. This enhancement is of great significance in practical applications with high noise levels.

3. Robustness to input noise level

In this section, the robustness of FRI to input noise level is also investigated. Figures 4(a) and 4(b) show the RMSEs of frequency and damping factor versus the bias of the MSE budget. Our FRI is robust to the inaccuracy of the input MSE budget. Note that, when the MSE budget is not small enough to break out of the loop, FRI runs for a fixed number of iterations and initializations and chooses the reconstruction that yields the minimum MSE.

4. Computation time

The effects of the number of sensors and samples on computation time for L2-CS, atomic-CS, and FRI are investigated in this part. L2-CS runs on 200 grids. As shown in Fig. 5, the computations time of L2-CS and atomic-CS increase rapidly with the number of samples and sensors. However, the computation time of our FRI is almost unchanged. FRI requires QR decomposition of matrices $\mathbf{A}_{i-1} \in \mathbb{C}^{NL\times(M+1)}$ and $\mathbf{B}_{i-1} \in \mathbb{C}^{NL\times ML}$ in Eq. (10), which can be performed at very low cost. Note that the matrix $\mathbf{B}_{i-1}$ is repetitive along the diagonal, so it only needs QR decomposition of a small matrix $\mathbf{R}_{i-1}\mathbf{U}_{N,M} \in \mathbb{C}^{N\times M}$. Therefore, the computation time of our FRI mainly scales with the number of sinusoids M but varies very slowly with the number of samples and sensors, as seen in Fig. 5. This allows us to process large amounts of real data in various real-time applications. On the other hand, the computation cost of standard techniques in ocean acoustics mainly depends on the number of samples N, which makes it difficult to satisfy the requirements of real-time applications (e.g., tracking, localization, etc.).

B. FRI sparse approximation in underwater acoustics

As shown in Fig. 6, the simulation setting are as follows. The density ρ_b, sound speed c_b, and attenuation α_b of sea bottom are 1.6 g/cm^3, 1584 m/s, and 0.2 $f^{0.8}$dB/λ, where f is frequency in kHz and λ is wavelength in meters. The depth of water is 60 m. The source emits a single-frequency signal at a depth of 30 m. Six sensors of VLA are at depths of 10, 20, 30, 40, 50, and 60 m. The source gradually moves away from the receiving array, and the range

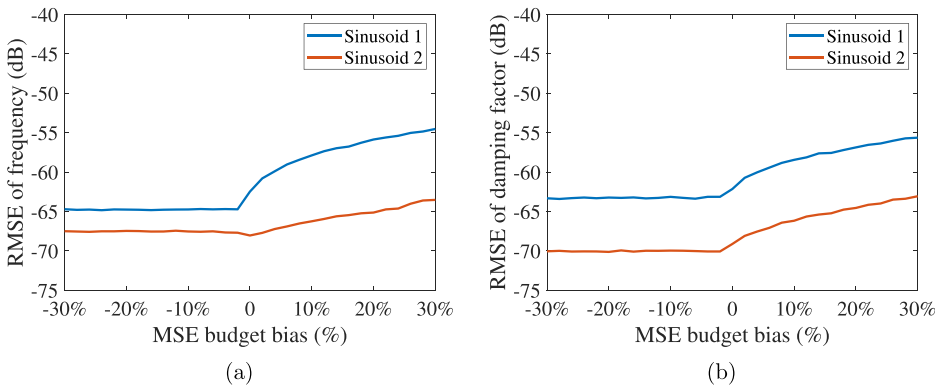

FIG. 4. (Color online) RMSE (averages over 10 000 random realizations) for FRI versus bias of the input MSE budget. Note $M = 2$ damped sinusoids, $N = 21$ samples, and $L = 3$ sensors (SNR = 20, 15, and 10 dB).

https://doi.org/10.1121/10.0016497

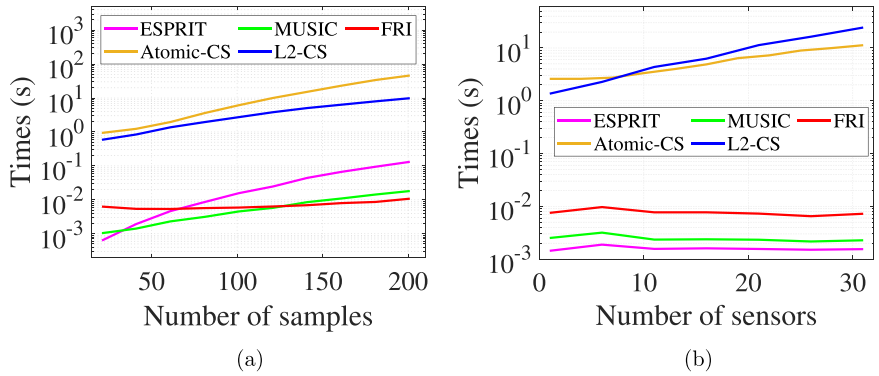

FIG. 5. (Color online) Computation time (averages over 1000 realizations) of ESPRIT, MUSIC, L2-CS, atomic-CS, and FRI versus (a) the number of samples N (the number of sensors $L = 3$) and (b) the number of sensors L (the number of samples $N = 21$). Note that $M = 2$ damped sinusoids, and SNR = 10 dB. The computational cost of FRI mainly depends on the model order M, in contrast with standard techniques in ocean acoustics which scale up with the number of samples N, becoming increasingly inefficient when larger amounts of data need to be processed.

sampling interval of the acoustic field is $\Delta r = 2$ m. The acoustic field is simulated with KRAKEN toolbox.[36] Note that, in this paper, what is known to us is only the spatial sampling interval Δr, in the absence of the range of source r. In simulations and experiments, we plot the range of source for ease of performance evaluation.

1. Wavenumber estimation

As for the mode wavenumber estimation, the common methods such as Fourier transform, MUSIC, L2-CS, and atomic-CS assume that the range of the source r is known to compute the cylindrical spreading $1/\sqrt{r}$.[2,3,6,18,21,22,29,30] They are not robust enough in the absence of the range of moving source.

Here, for visualization purpose, we calculate the ensemble amplitude $|c_m|$ associated with the m-th wavenumber by the incoherent superposition of each sensor

$$|c_m| = \sqrt{\frac{1}{L}\sum_{l=0}^{L-1} |c_{m,l}|^2}, \tag{16}$$

where $c_{m,l}$ is the amplitude associated with l-th sensor.

Figure 7(a) shows the estimation results of MUSIC, ESPRIT, L2-CS, Atomic-CS, and FRI at the source frequency of 100 Hz. The range is from 100 to 300 m with the sampling interval of 2 m. The common methods L2-CS, Atomic-CS, ESPRIT, and MUSIC are not able to retrieve all the three wavenumbers and also recover non-existing wavenumbers due to the absence of the range of the source and colored noise. FRI, instead, can locate all wavenumbers successfully by compensating for TL using damping factor α_m. It provides accurate and robust wavenumbers estimation with super-resolution.

In order to further verify the performance of the FRI algorithm, we test it at different source frequencies (50–100 Hz). Figure 7(b) shows the estimation results. Other simulation settings are the same as Fig. 7(a). Our FRI locates all wavenumbers accurately without knowing the range of the source.

2. Acoustic field reconstruction

The actual marine environment is complex due to the influence of winds, waves, tides, and currents. As a result, the underwater acoustic field is often corrupted by a strong environmental noise,[37–40] which seriously affects the subsequent processing.[41,42] In this part, we investigate the effectiveness of the parametric sparse representation, which approximates the acoustic field with a finite sum of damped sinusoids and recovers the acoustic field from the very noisy data.

As can be seen in Fig. 8, commonly used high-resolution methods are unable to achieve an accurate

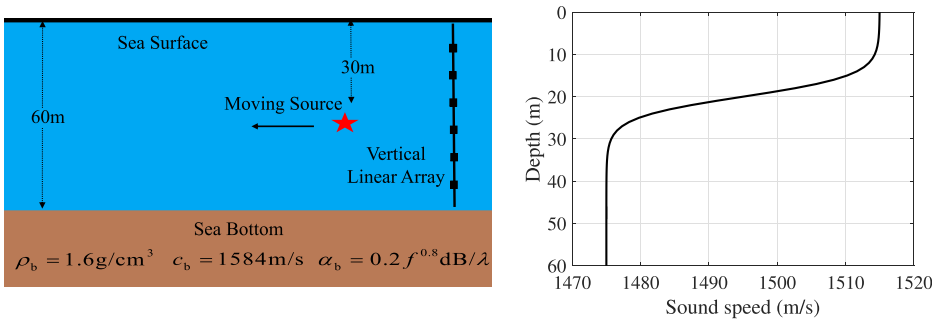

FIG. 6. (Color online) (a) Simulation environment schematic diagram. ρ_b, c_b, and α_b denotes the density, sound speed, and attenuation of sea bottom, where f is frequency in kHz and λ is wavelength in meter. A VLA is deployed at depths 10, 20, 30, 40, 50, and 60 m, respectively. A source that emits a single-frequency signal moves away from the VLA with range sampling interval 2 m. (b) Background sound speed profile.

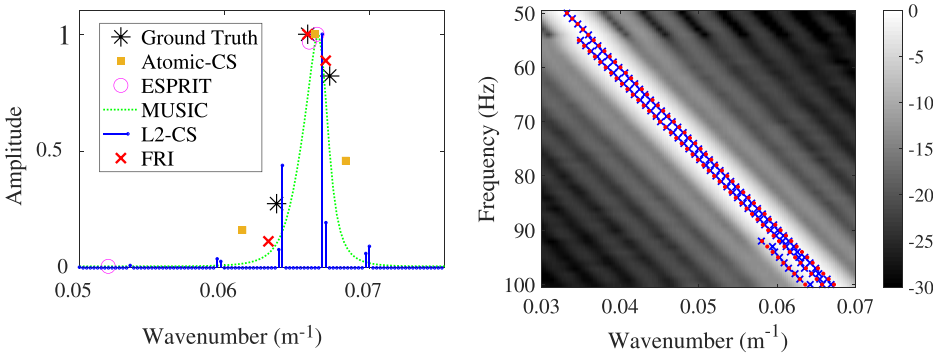

FIG. 7. (Color online) Estimation results of MUSIC, ESPRIT, L2-CS, atomic-CS, and FRI. The data consist of 6 sensors corrupted by colored noise SNR = 15 dB. The range is from 100 to 300 m with the sampling interval of 2 m. (a) Wavenumber estimation with source frequency 100 Hz. (b) Wavenumber estimation with source frequency 50–100 Hz. Background color represents the DFT. "•" denotes the ground truth. "×" denotes the estimated results by FRI. Because the wavenumbers are closely located, a robust high-resolution technique is required.

recovery of the acoustic field from the raw data due to the absence of the range of the source and intricate noise. Here, the range is set from 2000 to 7000 m with the sampling interval of 2 m and the source frequency is 100 Hz. Figure 9 shows details of the FRI recovery of acoustic field. FRI retrieves the hidden pure acoustic field from the raw data accurately, even in high noise levels: here, the SNR of the colored noise is −10 dB and yet the SNR of the FRI-recovered acoustic field is 20.71 dB. The single-sensor SNRs for raw data at depths of 10, 20, 30, 40, 50, and 60 m are −14.13, –9.78, –9.14, –10.30, –8.16, and −10.48 dB, respectively. After for FRI recovery, these SNRs become 16.73, 20.85, 24.84, 20.42, 21.80, and 18.64 dB, respectively. Our FRI provides an efficient representation and accurate recovery for the acoustic field.

3. Transmission loss estimation

Transmission loss (TL) describes the energy attenuation of the acoustic field underwater and plays an important role in sonar performance prediction.[1,43,44] It is defined as

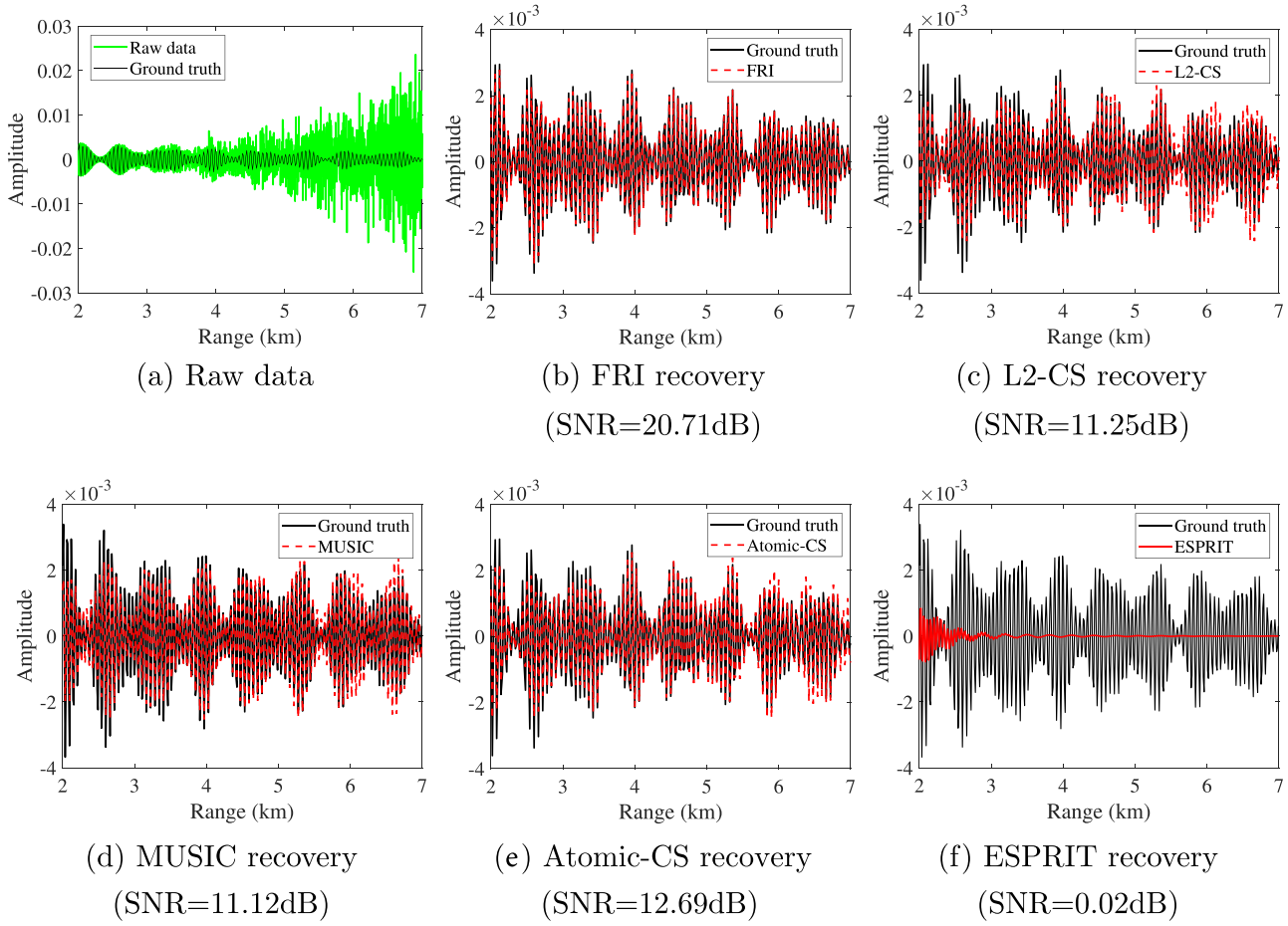

FIG. 8. (Color online) Reconstruction of a simulated acoustic field at source frequency 100 Hz. The raw data consist of 6 sensors with $N = 2500$ range samples (the range is from 2000 to 7000 m with a sampling interval of 2 m). The multi-sensor SNR of the raw data are –10 dB corrupted by colored and (inter-sensor) correlated noise. Only the raw data and the reconstructions at depth of 20 m are shown. Standard high-resolution methods in ocean acoustics are not robust enough to recover the acoustic field due to the intricate environmental noise. The energy of signal noise increases rapidly with range.

https://doi.org/10.1121/10.0016497

$$\mathrm{TL} = 20\log\left(\frac{|s(1,z_r)|}{|s(r,z_r)|}\right),$$

where the reference value (usually known) $s(1,z_r)$ is the acoustic amplitude at $r = 1$ m.

In this part, we investigate the effectiveness of approximating TL with damping factor α_m. Figure 10 indicates the TL at different depths with multi-sensor SNR $= -10$ dB. The simulation settings are same as Fig. 9. For the raw data, the acoustic propagation characteristics are completely buried under strong noise and it is hard to predict the sonar performance correctly. Our FRI compensates the TL well using the damping factor α_m instead of assuming that the range of the source is known. Applying the FRI approximation algorithm, we retrieve the TL accurately (multi-sensor SNR $=$ 19.81 dB). The raw single-sensor SNR at depths of 10, 20, 30, 40, 50, and 60 m are -14.17, –9.83, –9.12, –9.92, –8.61, and -10.33 dB, respectively. After FRI recovery, the single-sensor SNRs at depths of 10, 20, 30, 40, 50, and 60 m are 17.00, 19.18, 19.64, 21.53, 20.74, and 18.82 dB, respectively. Thanks to the robust FRI approximation, the energy loss of acoustic field can be accurately recovered, which is of particular interest in sonar detection.

V. SWELLEX-96 EXPERIMENT

In this section, the performance of our FRI approximation algorithm is further validated on real acoustic data collected from the complex shallow water environment. The raw data are acquired from the SWellEx-96 experiment Event S5 that was conducted near San Diego, CA in the spring of 1996. During the experiment, from 23:15 10 May to 00:30 11 May, two sources transmitting a unique set of tones in depths of about 9 and 54 m were towed from southwest to northeast. The data were collected by a 21-sensor VLA spanning in a depth from 94.125 to 212.25 m (sampling frequency $= 1500$ Hz). In this paper, we focus on the deeper source at a frequency of 49 Hz, with the range distance to the VLA changing from 8 to 3 km (see Fig. 11).

In practice, the signal is collected by sensors in time domain, and the time-range transformation is necessary as the acoustic field is characterized by the range and depth.[3,6,45] Assuming that the range between the source and VLA is invariant in a very short time (e.g., a duration of 3 s), the time signal can be transformed into range signal. This is a reasonable assumption as the underwater sound speed ($\approx$1500 m/s) is far larger than the speed of the source ($\approx$2.5 m/s).

Notice that the experiment involves a moving source with inadequate GPS data, which results in a large distortion of acquired acoustic measurements.[3,6,45] Moreover, the collected data are further corrupted by the intricate noise induced by marine environment (e.g., winds, tides/currents/waves and instrument noise[38–40]) As a consequence, it is quite challenging to recover the underlying acoustic field from the received data.

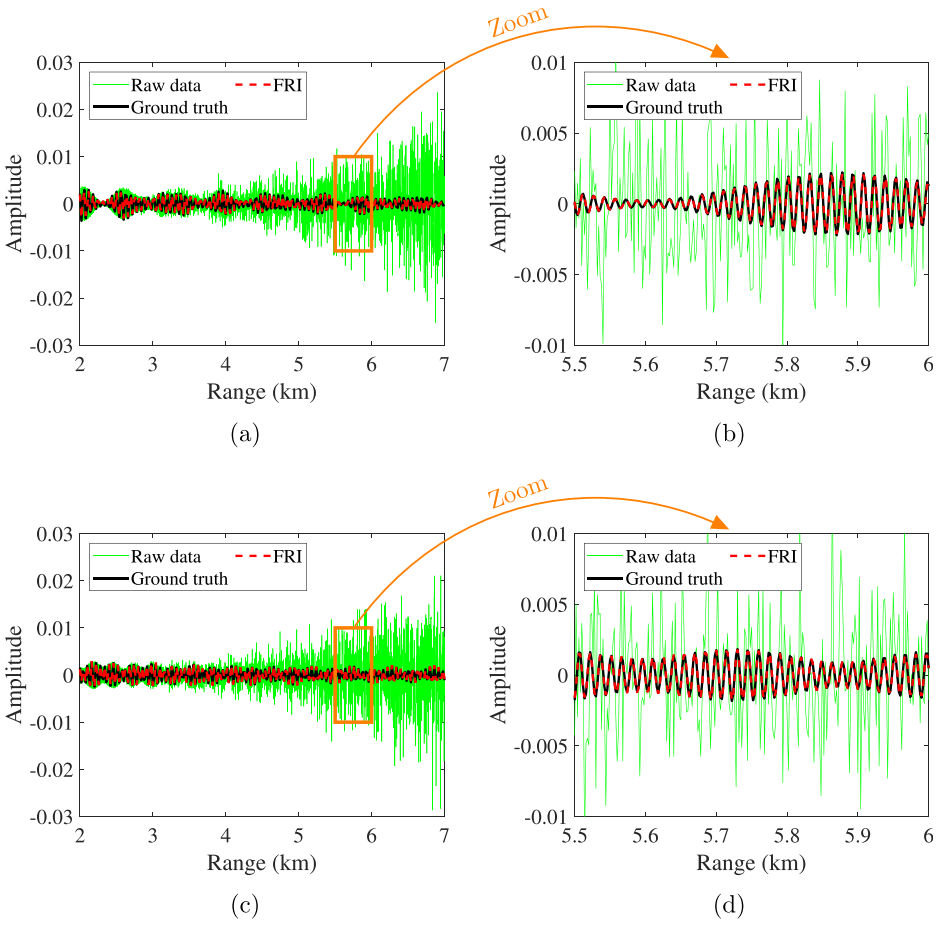

FIG. 9. (Color online) Details of the FRI reconstruction of the simulation described in Fig. 8. The run-time of the FRI algorithm is 0.3 s. Top row shows the reconstruction at a depth of 20 m, while the bottom row shows the reconstruction at 40 m. Contrary to the other high-resolution techniques, the acoustic field recovery provided by the FRI approach is sufficiently accurate to make it possible to calculate reliably the ocean parameters. The energy of signal noise increases rapidly with range.

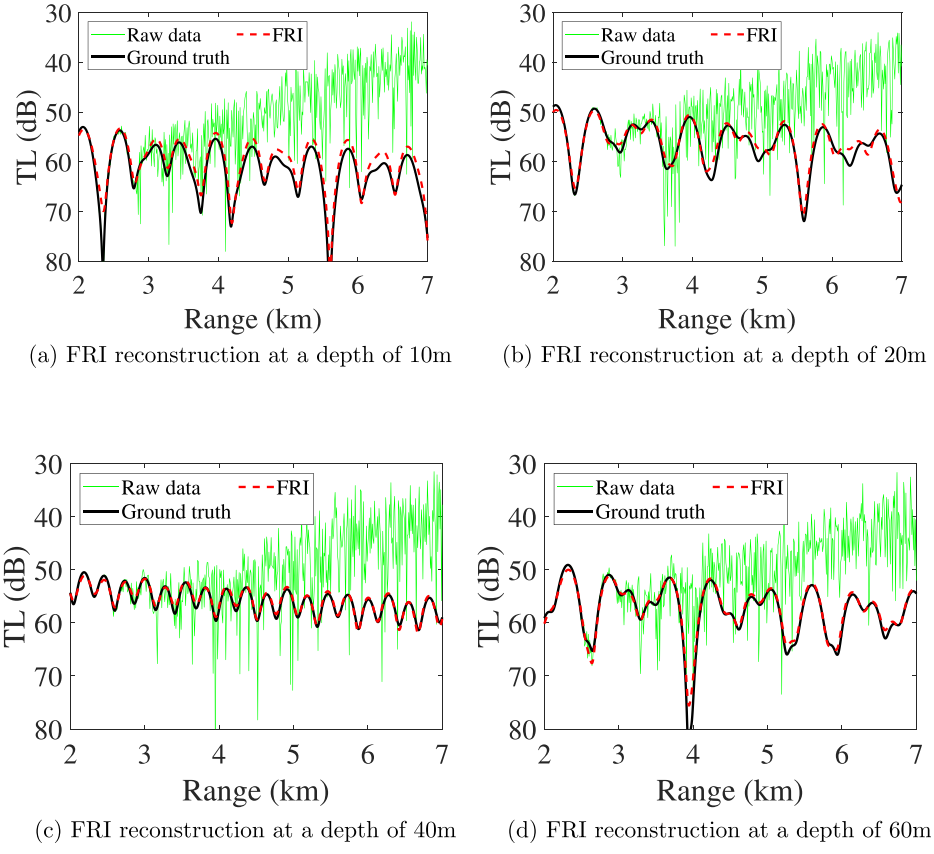

(a) FRI reconstruction at a depth of 10m (b) FRI reconstruction at a depth of 20m

(c) FRI reconstruction at a depth of 40m (d) FRI reconstruction at a depth of 60m

FIG. 10. (Color online) Reconstruction of the TL from simulated acoustic data: 6 sensors corrupted by intra- and inter-sensor correlated noise with multi-sensor SNR $= -10$ dB, range from 2000 to 7000 m with a sampling step of 2 m. The FRI reconstruction increases the multi-sensor SNR to 19.81 dB, for a run-time of about 0.3 s. The TL is an important parameter for detection applications.

Figure 12 shows the wavenumber estimation of FRI, ESPRIT, MUSIC, L2-CS, and atomic-CS on the real data (range from 8 to 3 km with an interval of 3.63 m). The reference wavenumbers are calculated by KRAKEN. Our FRI algorithm successfully locates six wavenumbers around the reference wavenumbers, despite the very intricate environmental noise caused by winds, tides/currents/waves, and instrument noise.[38–40] This demonstrates the performance of our FRI algorithm. Other high-resolution methods such as ESPRIT, MUSIC, L2-CS, and atomic-CS locate fewer reference wavenumbers but more outliers due to the absence of the range of the source and intricate noise.

Figures 13(a)–13(f) show the estimated mode shapes (i.e., amplitude $c_{m,l}$) by FRI from the real SWellEx-96 data. Despite the complex noise and inaccurate environment parameters, FRI successfully recovers the mode shapes that

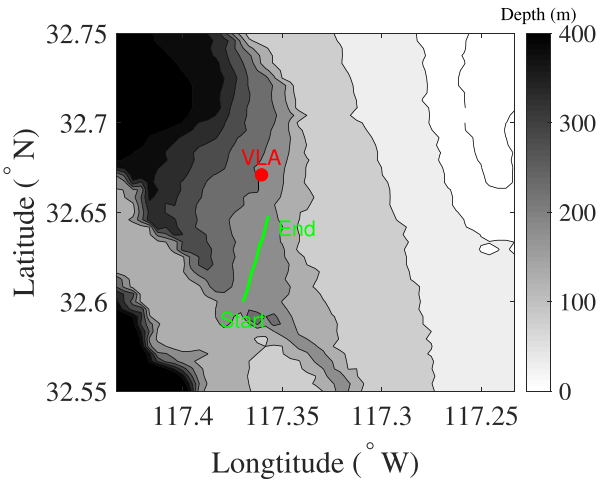

FIG. 11. (Color online) Illustration of the SWellEx-96 experiment. The towed source is moving along a trajectory (green line) at a speed of $v \approx 2.5$ m/s ($\ll$ underwater sound speed 1500 m/s). The range between the source and VLA (•) is from 8 to 3 km. The background color indicates the depth of water in the experimental area.

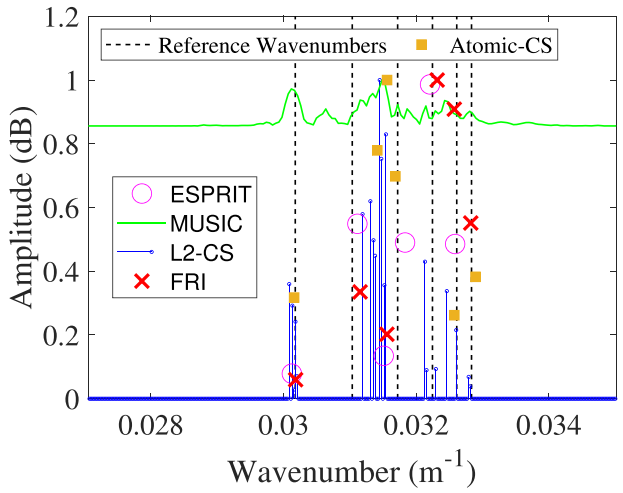

FIG. 12. (Color online) Wavenumber estimation of FRI, ESPRIT, MUSIC, L2-CS, and atomic-CS from noisy 21-sensor VLA measurements. Without knowing the ground truth values, reference wavenumbers are provided by KRAKEN.

https://doi.org/10.1121/10.0016497

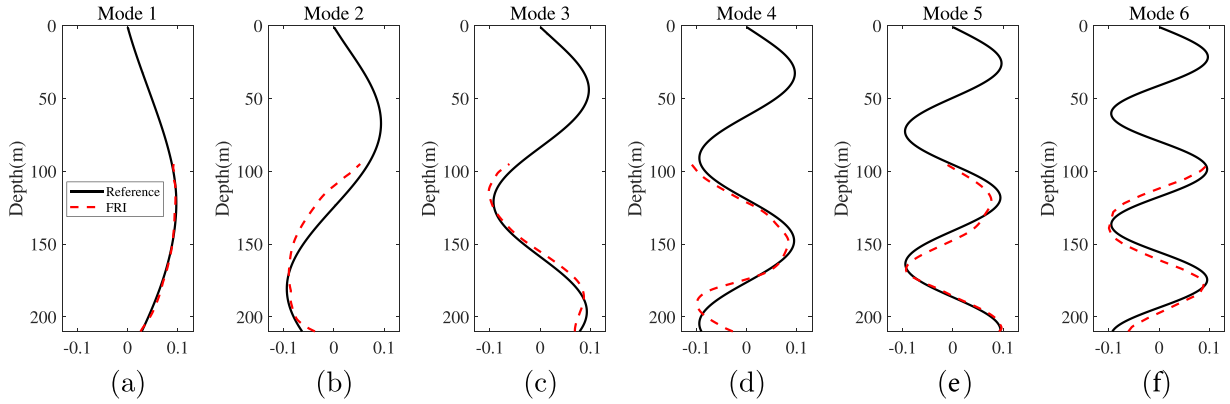

FIG. 13. (Color online) Mode shape reconstruction with SWellEx-96 data. The reference shapes associated with the reference wavenumbers are calculated by KRAKEN in Fig. 12.

match the reference shapes. This further verifies the effectiveness of FRI in real data.

Figure 14 shows the recovered acoustic field at depths of 212.25, 172.88, 122.25, and 111.00 m, respectively. The recovered acoustic fields are consistent with the predictions of ocean acoustics, as demonstrated in the wavenumber estimation of Fig. 12 and mode shape reconstruction of Fig. 13.

VI. CONCLUSION

In this paper, a method based on FRI is developed to recover an acoustic field from the VLA data, without knowing the range of the moving source. A joint sparse parametric model is proposed that approximates the attenuated field as a sum of damped sinusoids. By fitting data with the parametric model, our FRI achieves a robust and accurate recovery of the acoustic field by compensating for TL using the damping factor. However, other high-resolution is not robust enough to recover the acoustic field accurately due to the dependence on the range of the source and intricate noise. Dropping the noise stochastic assumptions, we propose the MSE criterion, which leads to an automatic and robust determination of model order. We demonstrate the performance of our FRI algorithm on simulations and real

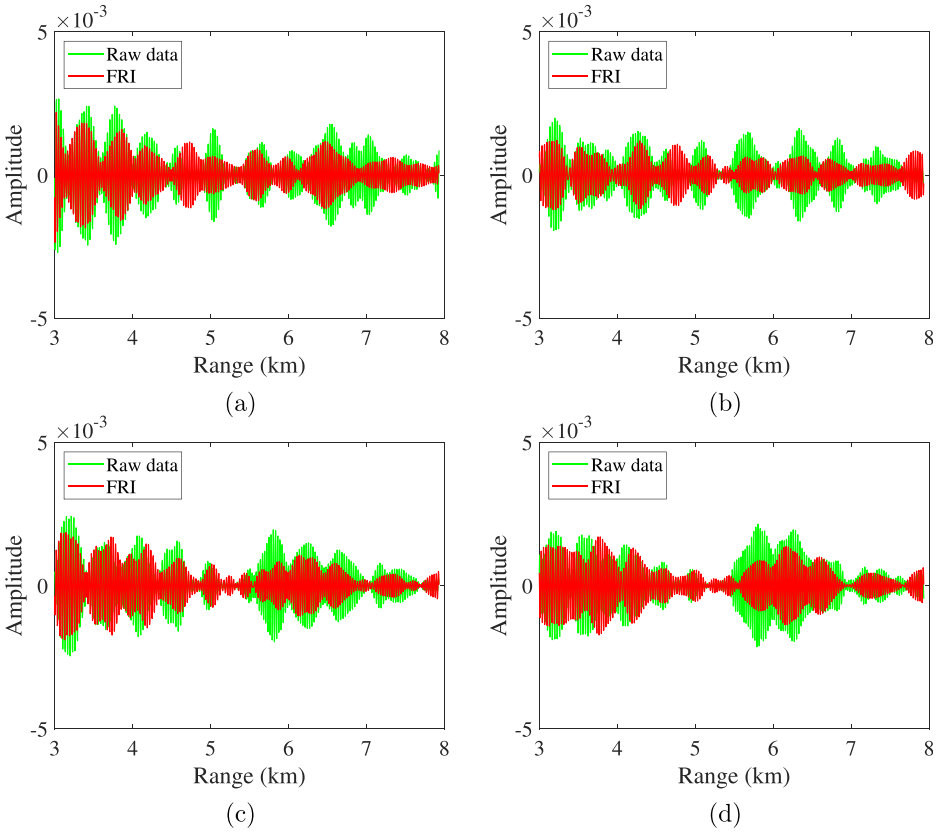

FIG. 14. (Color online) Acoustic field reconstruction from 21-sensor VLA data. (a)–(d) show the reconstructions at depths of 212.25, 172.88, 122.25, and 111.00 m. In particular, the accuracy of this reconstruction is corroborated by the ocean acoustic prediction shown in Figs. 12 and 13.

acoustic data. Moreover, this algorithm can be easily extended to more scenarios, e.g., multi-source environment, deep ocean, and high-frequency source environment.

ACKNOWLEDGMENTS

Y.L. and R.G. contributed equally to this work. This research was supported in part by the National Key R&D Program of China under Grant No. 2016YFC 1400100 and in part by the Science and Technology on Sonar Laboratory under Grant Nos. 6142109190202 and 6142109KF2018.

[1]F. B. Jensen, W. A. Kuperman, M. B. Porter, and H. Schmidt, *Computational Ocean Acoustics* (Springer, Berlin, 2011).
[2]F. Le Courtois and J. Bonnel, "Compressed sensing for wideband wavenumber tracking in dispersive shallow water," J. Acoust. Soc. Am. **138**(2), 575–583 (2015).
[3]Y. Park, P. Gerstoft, and W. Seong, "Grid-free compressive mode extraction," J. Acoust. Soc. Am. **145**(3), 1427–1442 (2019).
[4]H. Niu, P. Gerstoft, E. Ozanich, Z. Li, R. Zhang, Z. Gong, and H. Wang, "Block sparse Bayesian learning for broadband mode extraction in shallow water from a vertical array," J. Acoust. Soc. Am. **147**(6), 3729–3739 (2020).
[5]T. C. Yang, "Data-based matched-mode source localization for a moving source," J. Acoust. Soc. Am. **135**(3), 1218–1230 (2014).
[6]T. C. Yang, "Source depth estimation based on synthetic aperture beamfoming for a moving source," J. Acoust. Soc. Am. **138**(3), 1678–1686 (2015).
[7]T. Yang, "A method of range and depth estimation by modal decomposition," J. Acoust. Soc. Am. **82**(5), 1736–1745 (1987).
[8]J. Bonnel, C. Gervaise, B. Nicolas, and J. Mars, "Single-receiver geoacoustic inversion using modal reversal," J. Acoust. Soc. Am. **131**(1), 119–128 (2012).
[9]T. L. Poole, G. V. Frisk, J. F. Lynch, and A. D. Pierce, "Geoacoustic inversion by mode amplitude perturbation," J. Acoust. Soc. Am. **123**(2), 667–678 (2008).
[10]S. Walker, P. Roux, and W. Kuperman, "Focal depth shifting of a time reversal mirror in a range-independent waveguide," J. Acoust. Soc. Am. **118**(3), 1341–1347 (2005).
[11]H. Song, S. Kim, W. Hodgkiss, and W. Kuperman, "Environmentally adaptive reverberation nulling using a time reversal mirror," J. Acoust. Soc. Am. **116**(2), 762–768 (2004).
[12]E. Shang and Y. Wang, "Tomographic inversion of the El Nino profile by using a matched-mode processing (MMP) method," IEEE J. Ocean. Eng. **19**(2), 208–213 (1994).
[13]M. S. Ballard and K. M. Becker, "Inversion for range-dependent water column sound speed profiles on the New Jersey shelf using a linearized perturbative method," J. Acoust. Soc. Am. **127**(6), 3411–3421 (2010).
[14]Y. Li, R. Guo, T. Blu, and H. Zhao, "Generic FRI-based DOA estimation: A model-fitting method," IEEE Trans. Sign. Process. **69**, 4102–4115 (2021).
[15]R. Guo, Y. Li, T. Blu, and H. Zhao, "Vector-FRI recovery of multi-sensor measurements," IEEE Trans. Signal Process. 1 **70**, 4369–4380 (2022).
[16]B. Nicolas, J. Mars, and J.-L. Lacoume, "Geoacoustical parameters estimation with impulsive and boat-noise sources," IEEE J. Oceanic Eng. **28**(3), 494–501 (2003).
[17]T. B. Neilsen and E. K. Westwood, "Extraction of acoustic normal mode depth functions using vertical line array data," J. Acoust. Soc. Am. **111**(2), 748–756 (2002).
[18]G. V. Frisk and J. F. Lynch, "Shallow water waveguide characterization using the Hankel transform," J. Acoust. Soc. Am. **76**(1), 205–216 (1984).
[19]E. Shang, H. Wang, and Z. Huang, "Waveguide characterization and source localization in shallow water waveguides using the Prony method," J. Acoust. Soc. Am. **83**(1), 103–108 (1988).
[20]F. Le Courtois and J. Bonnel, "Autoregressive model for high-resolution wavenumber estimation in a shallow water environment using a broadband source," J. Acoust. Soc. Am. **135**(4), EL199–EL205 (2014).
[21]K. M. Becker and G. V. Frisk, "Evaluation of an autoregressive spectral estimator for modal wave number estimation in range-dependent shallow water waveguides," J. Acoust. Soc. Am. **120**(3), 1423–1434 (2006).
[22]S. D. Rajan and S. D. Bhatta, "Evaluation of high-resolution frequency estimation methods for determining frequencies of eigenmodes in shallow water acoustic field," J. Acoust. Soc. Am. **93**(1), 378–389 (1993).
[23]I.-T. Lu, R. C. Qiu, and J. Kwak, "A high-resolution algorithm for complex spectrum search," J. Acoust. Soc. Am. **104**(1), 288–299 (1998).
[24]Y. Chi, L. L. Scharf, A. Pezeshki, and A. R. Calderbank, "Sensitivity to basis mismatch in compressed sensing," IEEE Trans. Signal Process. **59**(5), 2182–2195 (2011).
[25]D. H. Chae, P. Sadeghi, and R. A. Kennedy, "Effects of basis-mismatch in compressive sampling of continuous sinusoidal signals," in *2010 2nd International Conference on Future Computer and Communication* (IEEE, New York, 2010), Vol. 2, pp. V2–739.
[26]G. Tang, B. N. Bhaskar, P. Shah, and B. Recht, "Compressed sensing off the grid," IEEE Trans. Inf. Theory **59**(11), 7465–7490 (2013).
[27]A. Xenaki and P. Gerstoft, "Grid-free compressive beamforming," J. Acoust. Soc. Am. **137**(4), 1923–1935 (2015).
[28]Y. Park, Y. Choo, and W. Seong, "Multiple snapshot grid free compressive beamforming," J. Acoust. Soc. Am. **143**(6), 3849–3859 (2018).
[29]J. B. Harley and J. M. Moura, "Dispersion curve recovery with orthogonal matching pursuit," J. Acoust. Soc. Am. **137**(1), EL1–EL7 (2015).
[30]Z. Li, H. Niu, Z. Gong, and R. Zhang, "Sparse Bayesian learning for horizontal wavenumber retrieval in underwater acoustical signal processing," in *2018 IEEE 23rd International Conference on Digital Signal Processing (DSP)* (IEEE, New York, 2018), pp. 1–4.
[31]P. Gerstoft, A. Xenaki, and C. F. Mecklenbräuker, "Multiple and single snapshot compressive beamforming," J. Acoust. Soc. Am. **138**(4), 2003–2014 (2015).
[32]C. Gilliam and T. Blu, "Fitting instead of annihilation: Improved recovery of noisy FRI signals," in *2014 IEEE International Conference on Acoustics, Speech and Signal Processing (ICASSP)* (IEEE, New York, 2014), pp. 51–55.
[33]C. Gilliam and T. Blu, "Finding the minimum rate of innovation in the presence of noise," in *2016 IEEE International Conference on Acoustics, Speech and Signal Processing (ICASSP)* (IEEE, New York, 2016), pp. 4019–4023.
[34]Y.-X. Yao and S. M. Pandit, "Cramér-Rao lower bounds for a damped sinusoidal process," IEEE Trans. Sign. Process. **43**(4), 878–885 (1995).
[35]E. Aboutanios and S. Ye, "Efficient iterative estimation of the parameters of a damped complex exponential in noise," IEEE Sign. Process. Lett. **21**(8), 975–979 (2014).
[36]M. B. Porter, "The Kraken normal mode program," Naval Research Lab, Washington, DC (1992).
[37]K. A. Abrahamsen, "Practical ship noise level measurements in shallow water," J. Acoust. Soc. Am. **146**(4), 3060 (2019).
[38]N. R. Chapman and A. Price, "Low frequency deep ocean ambient noise trend in the northeast pacific ocean," J. Acoust. Soc. Am. **129**(5), EL161–EL165 (2011).
[39]J. Berger, J.-R. Bidlot, M. Dzieciuch, W. Farrell, P. Worcester, and R. Stephen, "A deep ocean acoustic noise floor, 1–800 Hz," J. Acoust. Soc. Am. **143**(2), 1223–1233 (2018).
[40]D. K. Wilson, R. J. Greenfield, and M. J. White, "Spatial structure of low-frequency wind noise," J. Acoust. Soc. Am. **122**(6), EL223–EL228 (2007).
[41]L. T. Fialkowski, M. D. Collins, J. S. Perkins, and W. Kuperman, "Source localization in noisy and uncertain ocean environments," J. Acoust. Soc. Am. **101**(6), 3539–3545 (1997).
[42]A. B. Baggeroer, W. Kuperman, and H. Schmidt, "Matched field processing: Source localization in correlated noise as an optimum parameter estimation problem," J. Acoust. Soc. Am. **83**(2), 571–587 (1988).
[43]P. Gerstoft, C.-F. Huang, and W. Hodgkiss, "Estimation of transmission loss in the presence of geoacoustic inversion uncertainty," IEEE J. Oceanic Eng. **31**(2), 299–307 (2006).
[44]L. E. Kinsler, A. R. Frey, A. B. Coppens, and J. V. Sanders, *Fundamentals of Acoustics* (Wiley, New York, 2000).
[45]S. Walker, P. Roux, and W. A. Kuperman, "Modal doppler theory of an arbitrarily accelerating continuous-wave source applied to mode extraction in the oceanic waveguide," J. Acoust. Soc. Am. **122**(3), 1426–1439 (2007).